ACS APPLIED NANO MATERIALS

www.acsanm.org Article

Silica Surface Coating of Blue Light-Emitting $CsPbBr_3$ Nanoplatelets for Improved Stability in Polar Solvents and Long-Term Storage

Thi Kim Tran Tran, Hawi N. Nyiera, Courtney Brea, Sebastian Noguera Ruiz, Chao Wang, Haiyan Tan, Steven L. Suib, Guoxiang Hu, and Jing Zhao*

Cite This: *ACS Appl. Nano Mater.* 2024, 7, 12153−12162 Read Online

ACCESS | Metrics & More | Article Recommendations | Supporting Information

ABSTRACT: Colloidal quantum-confined perovskite $CsPbBr_3$ nanoplatelets (NPLs) exhibit blue emission, making them promising for blue LEDs. It is known that the thickness of $CsPbBr_3$ NPLs is not stable especially in polar solvents and during long-term storage, causing their absorption and emission to red-shift due to the transformation to a larger structure. To cope with this limitation, we developed a surface coating method to protect the NPLs. In particular, we designed a system to stabilize the thickness of NPLs during the silica coating process. We also explored the impact of functional groups of the capping ligands and reaction time on the spectroscopic performance of the NPLs to gain some insights into the surface passivation mechanism, which will benefit future shell growth methods using other materials, not only limited to silica. Under the optimal reaction conditions, a photoluminescence quantum yield of 81% was achieved for the silica coated $CsPbBr_3$ NPLs. These NPLs exhibited good stability in water and other polar solvents and after long-term storage. Density functional theory calculations show that the binding affinity of water on the NPL is decreased by silica coating. Based on the findings in this study, we proposed a mechanism of how a coating formed on the NPL surface to improve the stability and enhance the performance of $CsPbBr_3$ NPLs.

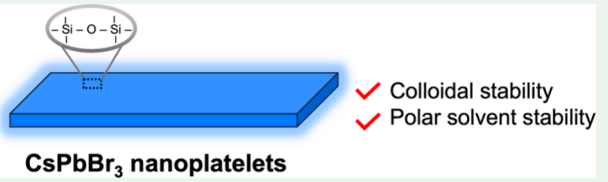

KEYWORDS: *$CsPbBr_3$ nanoplatelets, colloidal nanoparticle, blue-emitting materials, stability, surface coating*

INTRODUCTION

Colloidal lead halide perovskite nanocrystals (NCs) have demonstrated excellent optoelectronic properties, making them suitable for various applications such as solar cells,[1] photodetectors,[2] and light-emitting diodes (LEDs).[3] These NCs are known for their high photoluminescence (PL) quantum yield (QY) and narrow PL full width at half-maximum (fwhm) with easily tunable band gaps across a wide visible spectral range. They have the potential to be used in display applications, which require light emitting materials of the three primary colors: red (630−650 nm), green (520−530 nm), and blue (460−480 nm). Even though lead halide perovskite NC-based red- and green-emitting LEDs have achieved a remarkable success with external quantum efficiencies over 20%,[4,5] the NC-based blue LEDs are lagging behind in performance due to their low external quantum efficiencies and spectral and operational instabilities.[6,7] To address this challenge, it is necessary to obtain blue lead halide perovskite NCs with a high PL efficiency and stability.

Blue-emitting $CsPbX_3$ (X = Cl, Br, I, or a combination of them) NCs can be prepared by controlling either the halide composition or the NC size.[8] For the first approach, despite the ease to prepare mixed halide (e.g., $CsPb(Br_xCl_{1-x})_3$) NCs, they are subjected to irreversible phase segregation caused by ion migration, especially during device operation, leading to color instability.[9−11] In the second approach, the size of the $CsPbBr_3$ NCs is reduced below their Bohr exciton diameter (7 nm)[12] to make them either zero-dimensional (0D) or two-dimensional (2D) NCs. The size reduction increases their band gap due to quantum confinement, making them emitting in the blue spectral range. However, high quality blue-emitting 0D $CsPbBr_3$ NCs are difficult to obtain because the fast nucleation and growth process often cause size heterogeneity and broad emission; and they are easy to aggregate due to their high surface energy.[13] In contrast, the preparation of uniform blue-emitting 2D $CsPbBr_3$ nanoplatelets (NPLs) has been well established, although their stability is still not satisfying.[14−17] Thus, blue NPLs are adopted in this work, and surface modification is developed to improve their stability.

Similar to 3D $CsPbBr_3$ nanocubes, the conventional ligands oleylamine (OLA) and oleic acid (OA) are typically used for $CsPbBr_3$ NPLs synthesis. Previous work has shown that the Cs^+-to-OLA^+ molar ratio is the key factor to control the number of $CsPbBr_3$ monolayers in thickness.[17−20] However, those ligands have labile interactions with the surface of the $CsPbBr_3$ NPLs, which results in their easy desorption from the NPL surface. As a consequence, more surface defects and

Received: April 14, 2024
Revised: April 25, 2024
Accepted: April 28, 2024
Published: May 6, 2024

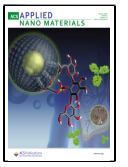

https://doi.org/10.1021/acsanm.4c02169
ACS Appl. Nano Mater. 2024, 7, 12153−12162

nonradiative recombination processes are induced in the NPLs, lowering their PLQYs.[21] The ligand detachment also leads to the instability of the NPLs against polar solvents, light, and elevated temperature, or even during storage.[22−24] Subsequently, the NPLs coalesce, causing the loss of quantum confinement; thus, the PL peak shifts from blue (450−470 nm) to green (500−520 nm). Both the surface defects and instability of blue-emitting $CsPbBr_3$ NPLs hinder their applications in optoelectronic devices.

Recently, several research groups have attempted to address some of these challenges. One approach is to utilize phosphonic acid and organic sulfate as ligands, which have strong binding affinity toward the $CsPbBr_3$ NPL surface to improve their PLQY and prevent NPLs to coalescence during storage.[14,25] Postsynthesis treatments with bromide additives can also effectively passivate surface bromide vacancies in $CsPbBr_3$ NPLs to enhance their PLQY, such as bromide ammonium-based salts,[15,16] $PbBr_2$,[18] $ZnBr_2$,[26] and bromide polysalt-$PbBr_2$ complex.[27] Regardless of the aforementioned progress, $CsPbBr_3$ NPLs exhibiting high PLQY and excellent stability against light, moisture, and polar solvents (which are usually used to purify NCs before device applications) still need to be developed.

Here, we developed a surface coating method to grow a silica coating on the $CsPbBr_3$ NPL surface to improve their stabilities against polar solvents and long-term storage. Ligand type, reaction time, and precursor ratios were considered in the synthetic design. The resultant NPLs exhibit enhanced PLQY up to 81% compared to that of the NPLs without the coating (11%). Also, their PL peak wavelength and spectral width remained unchanged after interaction with polar solvents and after long-term storage, proving the coating method helps prevent the coalescence of $CsPbBr_3$ NPLs.

EXPERIMENTAL SECTION

Chemicals. Lead(II) bromide ($PbBr_2$, 99.998% metals basis) was purchased from Thermo Scientific. Ammonium hydroxide (NH_4OH, 28.0−30.0%) solution was purchased from Baker Analyzed Reagent. Cesium carbonate (Cs_2CO_3, 99.9% trace metals basis), oleylamine (OLA, technical grade, 70%), oleic acid (OA, technical grade, 90%), (3-aminopropyl)triethoxysilane (APTES, 99%), hexadecyltrimethylammonium bromide (CTAB, ≥ 99%), isopropanol (IPA, ≥ 99.5%), octadecene (ODE, 90%), hexane (HPLC grade, ≥ 98.5%), and ethyl acetate (HPLC grade, ≥ 99.7%) were purchased from Sigma-Aldrich. All chemicals were used without further purification.

Synthesis of $CsPbBr_3$ NPLs. Cesium oleate solution (CsOA) was prepared by degassing 0.1625 g of Cs_2CO_3 in 5 mL of OA at 105 °C for 30 min to complete dissolution. CTAB/IPA solution was prepared by dissolving CTAB in IPA at a concentration of 3 mg/mL. A 15 μL portion of ammonia solution was added to 0.4 mL of IPA and CTAB/IPA solution to make NH_4OH/IPA and CTAB/NH_3/IPA solutions, respectively.

For pristine $CsPbBr_3$ NPLs (p-NPLs), 36.5 mg of $PbBr_2$, 0.25 mL of OA, 0.35 mL of OLA and 2 mL of ODE were added into a three-necked round-bottom flask and degassed at 65 °C for 30 min to completely dissolve $PbBr_2$. The solution was cooled to room temperature, and then 0.1 mL of cesium precursor was injected, followed by 0.25 mL of IPA. The reaction flask was transferred onto a hot plate preheated to 65 °C and kept there for 10 min. The synthesis of CTAB capped $CsPbBr_3$ NPLs is similar to that of the p-NPL, but 0.25 mL of CTAB/IPA solution was used instead of IPA.

Other than CTAB, APTES was also introduced during NPL synthesis. For CTAB-APTES-$CsPbBr_3$ NPL synthesis, 36.5 mg of $PbBr_2$, 0.25 mL of OA, 0.05 mL of OLA, 0.3 mL of APTES and 2 mL of ODE were added into a three-necked round-bottom flask and degassed at 65 °C for 30 min to completely dissolve $PbBr_2$. The solution was cooled to room temperature, and then 0.1 mL of cesium precursor was injected, followed by 0.25 mL of the CTAB/NH_3/IPA solution. The reaction flask was transferred onto a hot plate preheated to 65 °C and kept there for different reaction times at 10, 30, and 60 min. APTES-$CsPbBr_3$ NPLs were synthesized with similar procedure as CTAB-APTES-$CsPbBr_3$ NPLs at 30 min of reaction time, but the NH_3/IPA were used instead of CTAB/NH_3/IPA. Table 1 lists the sample notation.

Table 1. Sample Notation

Sample name	Reaction time (minutes)	Ligand composition during synthesis
10-CTAB-APTES-NPLs	10	APTES, CTAB, OA, and OLA
30-CTAB-APTES-NPLs	30	APTES, CTAB, OA, and OLA
60-CTAB-APTES-NPLs	60	APTES, CTAB, OA, and OLA
APTES-NPLs	30	APTES, OA, and OLA
CTAB-NPLs	10	CTAB, OA, and OLA
p-NPLs	10	OA and OLA

After allowing the reaction to proceed for the specified duration, the reaction mixture was cooled to room temperature with an ice−water bath, purified with ethyl acetate, volume ratio of reaction mixture to ethyl acetate as 1:6, and centrifuged at 7500 rpm for 10 min. The precipitate was collected and dispersed in hexane.

Instrumentation. Absorption spectra were collected by an Agilent Technologies Cary-60 UV−vis spectrometer. A Horiba FluoroMax Plus fluorometer equipped with an integrating sphere was used to collect PL spectra and QYs at an excitation wavelength of 350 nm. PL decay was measured by using a time-correlated single-photon counting (TCSPC) module (PicoHarp) with a pulsed laser excitation at 405 nm. High angle annular dark field scanning TEM (HAADF-STEM) images were obtained by a Thermo Fisher-Talos microscope at an accelerating voltage of 200 kV. X-ray powder diffraction (XRD) patterns were collected by a Bruker D2 Phaser with Cu Kα radiation. Fourier-Transform Infrared (FTIR) measurements were conducted with a Nicolet Magna 560 spectrometer. XPS (Thermo scientific K-Alpha) with an EX06 ion source was used to determine the surface composition of the samples. The quantification of the 1s, 2p and 4f peaks of N, Si, and Pb respectively was performed using casaXPS Version 2.3.26 software. Additionally, verification of charge problems was performed by locating the 1s peak of C, which was located around 285 eV for all samples, verifying that no correction for charge problems was required.

Theoretical Calculations. Spin-polarized density functional theory (DFT) calculations were performed using the Vienna *ab initio* simulations package (VASP).[28,29] The electron exchange-correlation was represented by the functional of Perdew, Burke and Ernzerhof (PBE) of generalized gradient approximation (GGA).[30] The ion-electron interaction was described with the projector augmented wave (PAW) method.[31] A cutoff energy of 400 eV was used for the plane-wave basis set. The energies were converged with a 1×10^{-4} eV tolerance, and the forces were optimized to within 0.03 eV/Å. The perovskite $CsPbBr_3$ NPLs were modeled with seven atomic layers with 2×2 supercells. The CsBr termination of the (100) surface was examined in this work. A vacuum of more than 20 Å along the *z*-direction was employed to avoid artificial interactions between images. The topmost three atomic layers of the NPLs, together with water/silica on the surface, were allowed to relax, while the bottom four atomic layers were kept frozen during the geometry optimizations. The binding energy of water was defined as $\Delta E = E_{total} - (E_{NPL} + E_{water})$, where E_{total}, E_{NPL}, and E_{water} correspond to the total energy of the NPL with water on the surface, the energy of the NPL, and the energy of an isolated water molecule, respectively. A more negative value of ΔE suggests a stronger binding.

https://doi.org/10.1021/acsanm.4c02169
ACS Appl. Nano Mater. 2024, 7, 12153−12162

RESULTS AND DISCUSSION

The method for synthesizing silica coated $CsPbBr_3$ NPLs (Scheme 1) was designed with careful consideration of the influence of precursors, solvents, and ligands on the stability of the NPLs during the silica coating process. Previous research has established that maintaining a rich bromide environment reduces the presence of Br^- vacancies on the perovskite surface and enhances QY.[32,33] Therefore, a $PbBr_2$ to Cs^+ ratio of 5:1 was selected to ensure an excess of bromide in the synthesis. Given the conventional OA and OLA ligands bind weakly to the perovskite surface with highly dynamic interactions, antisolvent purification or aging causes ligand detachment from the surface and thereby destabilizes the nanocrystals.[21] To mitigate this issue, CTAB was adopted because proton-free quaternary ammonium bromides have higher binding affinity to the perovskite surface and there is no proton exchange unlike primary ammonium bromides; as a result, they will remain attached to the perovskite surface, enhancing the stability of perovskite nanocubes.[34] Additionally, the CTA^+/Br^- ion pair can passivate the NPL surface at the A-site and Br^- vacancies, respectively. To further improve the stability of the NPLs against polar solvents and long-term storage, APTES was employed as the silica precursor in our synthesis to grow silica coating on the NPL surface. The amino group of APTES could incorporate into the surface A-site of the perovskite structure, while the ethoxysilyl groups ($-SiOC_2H_5$) would react to form Si−O−Si covalent bonds on the NPL surface. Lastly, considering the low solubility of CTAB in ODE (the solvent for NPL growth), IPA was used to dissolve CTAB and ammonium hydroxide solution was added to catalyze the silica growth. The reaction time for silica growth was varied to investigate its impact on the optical properties and stability of the resultant NPLs.

Scheme 1. Schematic Illustration of the Synthesis of CTAB-APTES-$CsPbBr_3$ NPLs

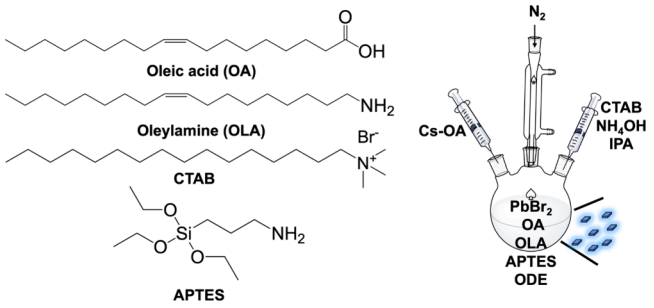

Figure 1a, b compares the UV−vis absorption and PL spectra of 30-CTAB-APTES-NPLs and CTAB-NPLs after purification using ethyl acetate. The 30-CTAB-APTES-NPLs have a thin silica coating on them whereas CTAB-NPLs do not. The absorption peak of 30-CTAB-APTES-NPLs was around 453 nm, slightly red-shifted in comparison with that of CTAB-NPL at 449 nm. These small changes could be due to the slight change in the thickness of the NPLs after coating, and/or changes in the surface ligands causing a different local dipole environment that slightly influences the absorption.[35] Both samples have similar emission peaks at 460 and 459 nm with and without silica coating, with PL fwhm values of 19 and 16 nm, respectively. TEM data in Figure 1 d and e confirmed that there was a remarkable difference in lateral dimension of the particles in the CTAB-NPL and 30-CTAB-APTES-NPL samples. This observation suggested that the silica coating impacted the lateral size of the NPLs and therefore improved their solubility. It also explained the reason why the growth solution is transparent for 30-CTAB-APTES-NPLs but opaque for CTAB-NPLs (see inset in Figure 1a). CTAB-NPLs with large lateral dimensions are hard to disperse in solution. Additionally, TEM results indicated a slight increase in the

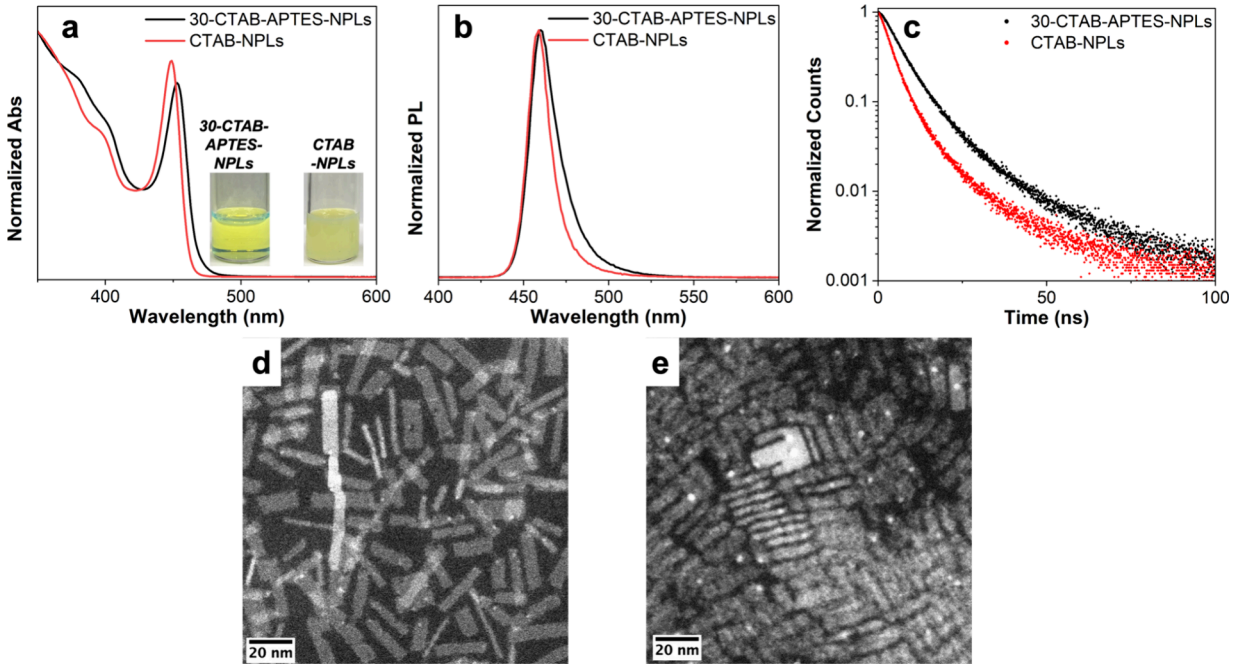

Figure 1. (a) Absorption, (b) PL spectra, and (c) lifetime of 30-CTAB-APTES-NPLs and CTAB-NPLs (measured using samples with the same optical density at 450 nm). The inset in Figure 1a shows images of the reaction solution after synthesis for 30-CTAB-APTES-NPLs (left) and CTAB-NPLs (right). (d, e) HAADF-TEM images of 30-CTAB-APTES-NPLs and CTAB-NPLs.

https://doi.org/10.1021/acsanm.4c02169
ACS Appl. Nano Mater. 2024, 7, 12153−12162

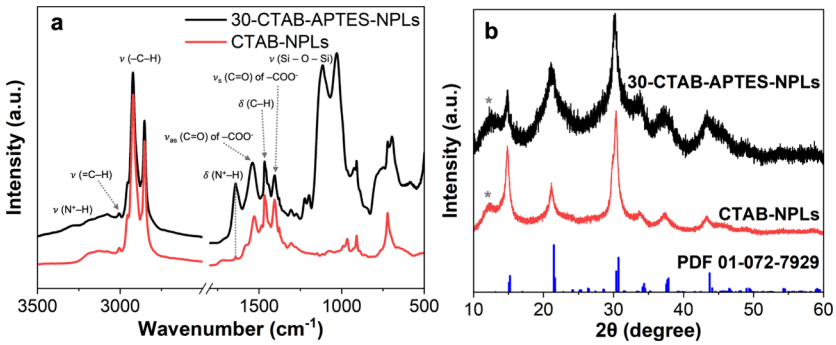

Figure 2. (a) FTIR spectra (taken after sample purification) and (b) XRD patterns of 30-CTAB-APTES-NPLs and CTAB-NPLs.

thickness of 30-CTAB-APTES-NPLs (2.6 ± 0.3 nm) compared with CTAB-NPLs (2.7 ± 0.4 nm). Even though there is a bit difference in the thickness from TEM, based on the PL peak position, the thickness of both samples should be 5 unit cells.[17] Moreover, there was a significant increase in the PLQY of 30-CTAB-APTES-NPLs to 81 ± 5% compared to that of CTAB-NPLs of 11 ± 0.6%. The PL decay of the two samples was fitted with a biexponential decay function:

$$I(t) = A_1\exp\left(\frac{-t}{\tau_1}\right) + A_2\exp\left(\frac{-t}{\tau_2}\right) + y_0$$

The average lifetime is determined by

$$\tau_{avg} = \left(\frac{(A_1\tau_1^2) + (A_2\tau_2^2)}{(A_1\tau_1) + (A_2\tau_2)}\right)$$

where τ_i is the lifetime of the ith decay component and A_i is a weighting coefficient of that component.

The average PL lifetime of 30-CTAB-APTES-NPLs was determined to be 14.3 ns, higher than that of CTAB-NPLs of 10.7 ns. The increase in QY and lifetime implies a reduction of the nonradiative decay rate of 30-CTAB-APTES-NPLs. We attribute it to better passivation of the NPL surface by amino functional groups of APTES either occupying the A-site vacancies or binding to surface Br^- ions, resulted in reduction of the surface defect states.[35] We also notice a slight broadening of the PL spectrum of 30-CTAB-APTES-NPLs compared to that of CTAB-NPLs, in particular at the low-energy side (480−500 nm). Similar phenomenon has been observed in perovskite materials with local structural disorder resulting from either structure imperfections or doping,[36] also in ultrasmall perovskite quantum dots with high density of localized surface states.[37] Here, the peak broadening can be ascribed to the amino passivation and the formation of Si−O−Si covalent bonds on the NPL surface, which may partially disorder the NPL surface structure to form local potential energy fluctuation and then created localized exciton trap states.[36] The excitons trapped in these states can undergo radiative recombination to emit light on the low-energy side (480−500 nm).[36,37]

FTIR spectroscopy was used to study the surface chemistry of $CsPbBr_3$ NPLs and to confirm the silica formation on the NPL surface. In Figure 2a, FTIR spectra of both 30-CTAB-APTES-NPLs and CTAB-NPLs show the presence of ammonium with N^+−H stretching and bending vibrations at 3123 and 1640 cm^{-1}, respectively.[38] However, CTAB-NPLs had a much weaker N^+−H bending absorption than 30-CTAB-APTES-NPLs, probably because fewer ammonium groups were present on the surface of CTAB-NPLs than 30-CTAB-APTES-NPLs. Vibrational peaks at 1540 and 1405 cm^{-1} corresponding to asymmetric and symmetric stretches of C═O of $-COO^-$ confirmed OA attachment on the surface of both samples.[39] Asymmetric and symmetric C−H stretches in the hydrocarbon chains of the ligands were also observed at 2921 and 2852 cm^{-1}. Moreover, strong peaks at 1115 and 1030 cm^{-1} in the IR spectrum of 30-CTAB-APTES-NPLs due to the Si−O−Si stretching vibration verified silica coating formed on these NPLs. Additionally, the peak of Si (2p) observed in the XPS spectra of CTAB-APTES-NPL samples also confirmed the presence of silica coating on the $CsPbBr_3$ NPL surface, as shown in Figure S1. XPS analysis in Table S1 compares the Si/Pb and N/Pb ratios for different samples with different reaction times. Out of the CTAB-APTES-NPL samples, the 10 min sample has higher ratios of N/Pb and Si/Pb than the 30 min sample, which indicates the presence of more unreacted APTES molecules and other amine-based ligands. However, when the reaction time increased from 30 to 60 min, the reduction of N/Pb ratios (from 0.087 to 0.063) along with the increase of Si/Pb ratios (from 0.075 to 0.088) suggests that higher amount of silica formed on NPL surface while other amine-based ligands desorbed.

To determine the crystal structure of the NPLs with and without silica coating, XRD measurements were conducted on the NPLs drop-casted and dried on glass slides. The XRD patterns of 30-CTAB-APTES-NPLs and CTAB-NPLs are shown in Figure 2b and both of them have the orthorhombic phase structure (the broad peaks at 12.5° denoted by asterisk signs are resulted from the glass slide). Compare with the reference of bulk $CsPbBr_3$ orthorhombic crystal structure, the diffraction peaks shifted slightly to lower angle due to perovskite lattice expansion in 2D structures.[40,41] Three major peaks at 14.8°, 21.1°, and 30.3° correspond to (110), (020), and (220) planes. In contrast to the XRD peaks of CTAB-NPLs, the peaks of 30-CTAB-APTES-NPLs are broader and the intensity of the 21.1° peak intensity is much higher. This phenomenon was caused by a more random stacking of NPLs and was also reported in polymers coated $CsPbBr_3$ NPLs.[27]

In the silica coating procedure developed here, we hypothesize that CTAB is responsible for stabilizing the $CsPbBr_3$ NPLs and maintaining their original thickness during the synthesis of silica-coated $CsPbBr_3$ NPLs. To verify the role of CTAB, we synthesized $CsPbBr_3$ NPLs with different ligand compositions and reaction times. Without CTAB, the APTES-NPLs exhibited an absorbance peak at 454 nm with a shoulder at 471 nm and two emission peaks at 458 and 474 nm (Figure 3a), indicating that the sample contains NPLs with different

https://doi.org/10.1021/acsanm.4c02169
ACS Appl. Nano Mater. 2024, 7, 12153−12162

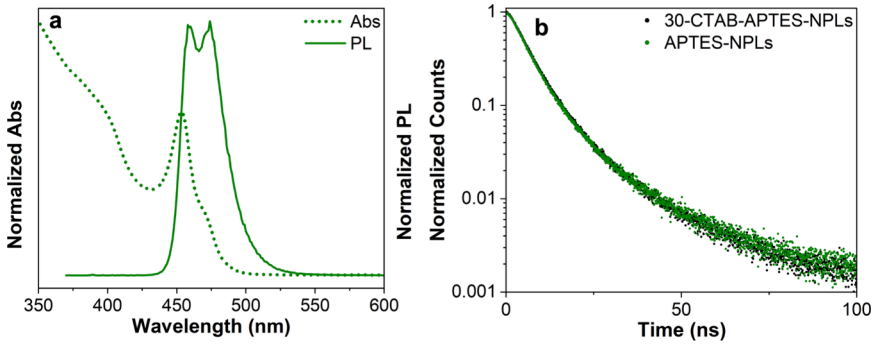

Figure 3. (a) Exclusion of CTAB in the synthesis changed the absorption and PL spectra of APTES-NPLs. (b) PL decays of 30-CTAB-APTES-NPLs and of APTES-NPLs.

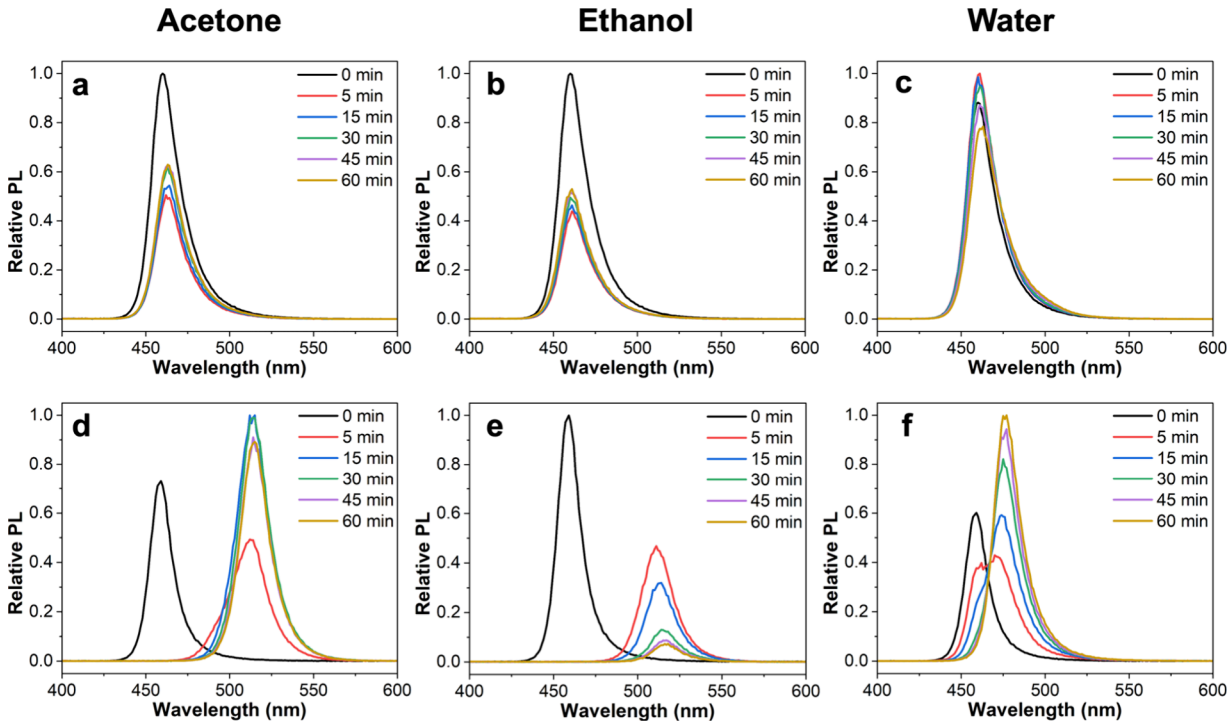

Figure 4. Chemical stability of (a–c) 30-CTAB-APTES-NPLs and (d–f) CTAB-NPLs against polar solvents (from left to right: acetone, ethanol, and water).

thicknesses of 3.3 and 2.9 nm, determined by TEM (Figure S2). Compared to 30-CTAB-APTES-NPLs, APTES-NPLs had a slightly higher PLQY of 86%, likely because the emission of thicker NPLs is less susceptible to surface defects. Their PL decays in Figure 3b almost overlapped with each other, suggesting no significant difference in their PL lifetimes. FTIR and XRD data (Figure S3) displayed no remarkable difference in all samples in terms of surface chemistry and crystal structure. We also found that for p-NPLs in which only OA and OLA were used as surface ligands, the absorption and emission peaked at 444 and 452 nm (Figure S4), respectively, in agreement with TEM results which suggested their thickness of 2.3 nm or 4 unit-cells.[17] Hence, the presence of CTAB during the synthesis maintains the NPL thickness during silica coating. Moreover, we varied the silica growth time of the CTAB-APTES-NPL samples for 10, 30, and 60 min to evaluate the effect of reaction time on the resulting NPLs. There was no change in absorption and PL spectra of these samples with the peaks at 453 and 460 nm, respectively (Figure S4). In addition, TEM results suggested the same thickness of 5 unit-cells for all these samples. 30-CTAB-APTES-NPLs had the highest PLQY of 81 ± 5% compared to the ones of 10- (67 ± 4%) and 60-CTAB-APTES-NPLs (64 ± 1%). This QY difference could be due to the difference in surface passivation at different reaction times, which also affects the stability of the NPLs.

To examine how silica coating improves the chemical stability of $CsPbBr_3$ NPLs, the PL intensities of 30-CTAB-APTES-NPL and CTAB-NPL samples were monitored with the addition of acetone, ethanol and water at 10% in volume to hexane solutions of NPLs (Figure 4, Figure S5, and Table S2). The PL spectra at 0 min were taken in pure hexane, and the concentrations of NPLs in pure hexane or hexane/polar solvent mixtures were kept the same. The PL peak wavelengths of all the CTAB-APTES-NPL samples had almost no change with the addition of acetone and ethanol. However, the PL intensity decreased very quickly after acetone or ethanol was added. 30-CTAB-APTES-NPLs showed PL intensity decrease of 37% or 47% after exposure to acetone or ethanol for 60 min. When water was added, 30-CTAB-APTES-NPLs showed no change in emission wavelength but an intensity loss of 11%

https://doi.org/10.1021/acsanm.4c02169
ACS Appl. Nano Mater. 2024, 7, 12153−12162

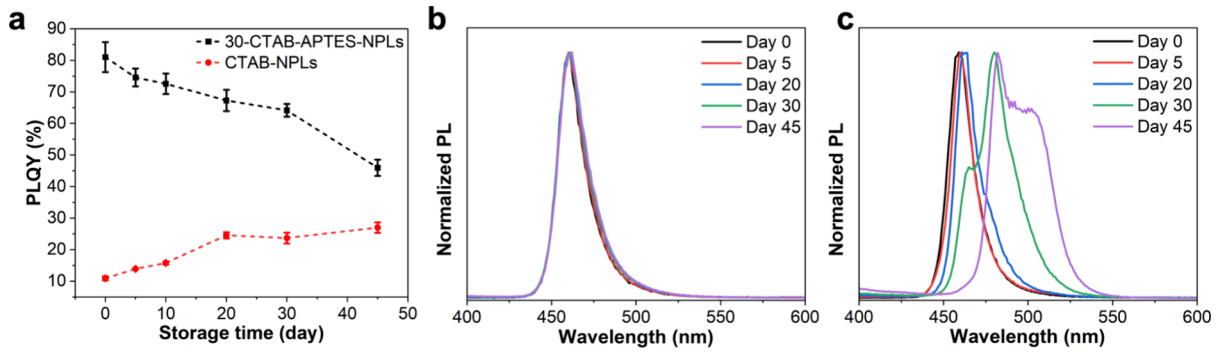

Figure 5. Stability of 30-CTAB-APTES-NPLs and CTAB-NPLs after long-term storage in ambient conditions: (a) PLQY and (b, c) PL spectra of 30-CTAB-APTES-NPLs and CTAB-NPLs, respectively.

after 60 min. In contrast, the emission wavelength of 10-CTAB-APTES-NPLs and 60-CTAB-APTES-NPLs red-shifted to 480 nm and the intensity was reduced by 39% and 59%, respectively, after 60 min of exposure to water (Figure S5). This phenomenon indicates that 30 min reaction time yields the best surface passivation of the NPLs and makes them less susceptible to water. The best surface passivation also leads to the highest PLQY of 30-CTAB-APTES-NPLs compared to that of the samples with 10 and 60 min reaction times. A similar PL intensity decrease was found for APTES-NPLs without CTAB capping ligands; but their PL spectral shape and wavelength changed in the polar solvents, especially in water, suggesting that a morphology change occurred. Therefore, CTAB is required to maintain their postsynthesis morphology. These observations suggest that the silica coating on the NPLs provides some protection against polar solvents.

In the control experiments with CTAB-NPLs and p-NPLs, their emissions red-shifted to above 500 nm in acetone and ethanol and to above 470 nm in water after only 5 min exposure to these solvents (Figure S5). The red-shifts were due to the transformation of the NPLs to bigger nanostructures driven by the presence of solvents with high polarity, resulting in a loss of quantum confinement.[22] The PL intensity increased after CTAB-NPLs and p-NPLs were exposed to acetone and water for some time but reduced significantly in ethanol. It is known that polar solvents cause rapid ligand detachment from $CsPbBr_3$ nanocube surface and increase surface defects which leads to emission reduction or even disassembly of perovskite structures.[21] But in some other events, appropriate amount of polar solvents can change the crystallization environment and induce reconstruction of the crystals to form different shapes and even enhance the emission.[42] Here, the solubility of $CsPbBr_3$ NPLs as well as ligands is different in different polar solvents; thus, ligand detachment and reconstruction of the crystal structure were impacted differently, leading to the discrepancy in the PL properties.

We also examined the stability of $CsPbBr_3$ NPLs during extended storage under ambient conditions, which is a significant concern because of their susceptibility to humidity-induced damage. The NPL samples were stored in transparent glass vials on the lab bench, and their PL QYs and spectra were monitored over an extended period. It was found that all of CTAB-APTES-NPL samples exhibited a similar trend in PLQY change over time. And all of their emission peaks and fwhm values remained the same over 45 days (Figure 5 and Figure S6). The PL QY of 30-CTAB-APTES-NPLs dropped from 81% to 46% after 45 days of storage. PLQY of APTES-NPLs reduced from 86% to 42% with an increase in the intensity of the peak at 474 nm, but a decrease in the one at 458 nm peak. This spectral change is consistent with that observed when the sample was exposed to water. It indicates that the NPLs had transformed into bigger nanostructures. This transformation was also observed in CTAB-NPLs and p-NPLs after storage (Figure S7). Notably, the emission peak of CTAB-NPLs slightly red-shifted by 4 nm after 20 days; while for p-NPLs, their emission spectrum had a remarkable redshift of 39 nm. The much smaller peak shift in CTAB-NPLs confirms again the power of CTAB in maintaining the thickness of the $CsPbBr_3$ NPLs. After 45 days, the PL spectrum of CTAB-NPLs became broader and the peak was shifted to 482 nm with a shoulder at 502 nm indicating the loss of quantum confinement. Moreover, the PLQY CTAB-NPLs and p-NPLs became higher over time. The increase in PLQY is ascribed to NPL reconstruction to form bigger perovskite NCs, which have lower surface-area-to-volume ratio and their emission is less affected by surface defects. The improved spectral stability of the silica coated NPLs demonstrates that our surface coating method has successfully prevented NPLs from coalescence over time. Note that although the silica coating effectively prevented the NPLs from aggregation, even at 55 °C (Figure S8), the PL intensity of the 30-CTAB-APTES-NPLs decreases after exposure to UV light, which is presumably due to some damage of the surface passivation caused by UV light (Figure S9).

The surface coating method we developed involves the interaction of ligands toward the $CsPbBr_3$ surface and sufficient reaction time for Si−O−Si bond formation with a proposed mechanism as illustrated in Figure 6. Ligands used to passivate the NPL surface included OA, OLA, CTA^+Br^- and the amino group of APTES. After 10 min of reaction, the ligands attach on NPL surface while ethoxysilyl groups ($-SiOC_2H_5$) undergo hydrolysis and condensation catalyzed by ammonia to create Si−O−Si covalent bonds. Previous studies have shown that the formation of silica coating on different types of materials is subjected to reaction time, so that one can control the thickness and uniformity of silica shell by varying the reaction time.[43−47] Here, 10 min reaction time is insufficient to complete the coating on the $CsPbBr_3$ surface, so there is not enough boundary to separate the polar solvents and prevent them from destructing the NPLs. With 30 min of reaction time, silica growth progresses further and more Si−O−Si covalent bonds are formed. Meanwhile, the passivation ligands are still attached to the $CsPbBr_3$ NPL surface. Thus, the surface coating better protects the NPLs from their

https://doi.org/10.1021/acsanm.4c02169
ACS Appl. Nano Mater. 2024, 7, 12153−12162

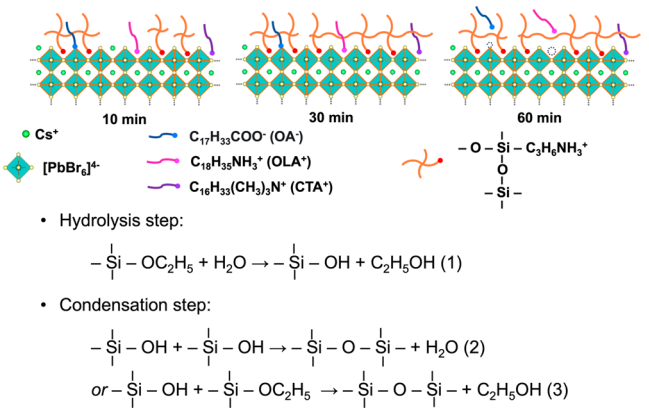

Figure 6. Mechanistic model of the surface coating approach to protect NPLs from coalescence.

surroundings (e.g., water) and improves the PLQY of the NPLs. When reaction time further increases to 60 min, the formation of the Si−O−Si covalent bonds is completed and a high coverage of the silica coating is achieved. This would prevent the highly dynamic ligands from coming back to the surface and causing defects on the surface. This makes NPLs more easily damaged by polar solvents and lowers the PLQY value. These observations are in line with a previous study showing that surface ligands were detached during silica encapsulation process causing a lower PL intensity from $CsPbBr_3$ nanocubes.[48] Furthermore, due to the potential random cross-linking of the NPLs caused by Si−O−Si formation,[49] a ligand with high binding affinity to the perovskite surface, i.e., CTAB, not only helps to maintain the NPL thickness during the synthesis but also prevents agglomeration of the NPLs. This mechanistic study gains insights into the silica formation process on the $CsPbBr_3$ surface.

We performed first-principles DFT calculations to provide a fundamental understanding of the change in stability against water for $CsPbBr_3$ NPLs with and without a silica coating. We first calculated the binding energy of water on the bare $CsPbBr_3$ NPL without organic ligands or silica. We found that the water molecule interacted strongly with the NPL surface, and the binding energy was −0.57 eV. As shown in Figure 7b, two hydrogen bonds were formed between the hydrogen atoms of water and surface bromine atoms. In addition, the water molecule interacted with the surface via the lone pair of the oxygen atom, and the Cs−O bond length was 3.078 Å (not shown in the figure). The strong binding affinity of water on the bare NPL provided an atomistic-level explanation for the low stability against water for 10-CTAB-APTES-NPLs, where the NPL surfaces were not well coated by silica. We then calculated the binding energy of water for silica coated $CsPbBr_3$ NPLs. As shown in Figure 7c, we found the binding of water was weak (binding energy = −0.21 eV) when both silica and hydrophobic ligands (e.g., OLA^+) are present on the NPL surface.[51] This suggests a good water repelling ability/moisture resistance,[50] and explained the improved stability for 30-CTAB-APTES-NPLs from experiments. As for the NPL surface only covered by silica, we found the binding affinity of water becomes stronger (binding energy = −0.36 eV). This can be attributed to the surface defect formation caused by desorption of hydrophobic ligands from the surface. Our computational results are in line with the experimentally observed lower stability against water for 60-CTAB-APTES-NPLs in comparison with 30-CTAB-APTES-NPLs.

CONCLUSIONS

We developed a surface coating synthesis to protect blue-emitting $CsPbBr_3$ NPLs, enhancing their stability against damage from polar solvents and coalescence during storage. The method produced NPLs with high PLQY of 81% and preserved their orthorhombic crystal structure. Multiple stability tests were performed to examine the impact of silica coating as well as to understand the function of ligands and the effect of reaction conditions for coating efficiency. CTAB ligands were identified as a major factor to maintain the NPL thickness unchanged during the synthesis in bromide-rich condition. And the reaction time was found to change the silica coating quality, thus affecting the stability of the NPLs. This study will contribute to the development of stable $CsPbBr_3$ NPLs for light emitting applications. The surface coating method can also be applied to improve the stability of other types of halide perovskite materials.

ASSOCIATED CONTENT

Supporting Information

The following files are available free of charge. The Supporting Information is available free of charge at https://pubs.acs.org/doi/10.1021/acsanm.4c02169.

Additional absorption, PL, XPS, XRD, FTIR, and TEM data (PDF)

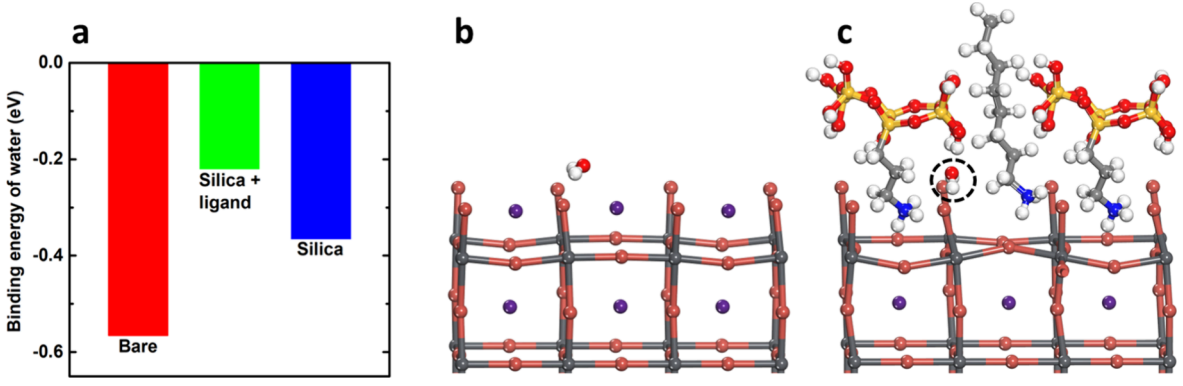

Figure 7. (a) Binding energy of water on perovskite $CsPbBr_3$ NPLs. Optimized atomic structures for the binding of water on NPLs (b) not coated with silica and (c) coated with silica. H, white; C, gray; N, blue; O, red; Si, yellow; Br, brown; Cs, purple; Pb, dark gray.

https://doi.org/10.1021/acsanm.4c02169
ACS Appl. Nano Mater. 2024, 7, 12153−12162

AUTHOR INFORMATION

Corresponding Author

Jing Zhao − *Department of Chemistry, University of Connecticut, Storrs, Connecticut 06269-3060, United States;* orcid.org/0000-0002-6882-2196; Email: jing.zhao@uconn.edu

Authors

Thi Kim Tran Tran − *Department of Chemistry, University of Connecticut, Storrs, Connecticut 06269-3060, United States*

Hawi N. Nyiera − *Department of Chemistry, University of Connecticut, Storrs, Connecticut 06269-3060, United States*

Courtney Brea − *Department of Chemistry and Biochemistry, Queens College of the City University of New York, New York, New York 11367, United States*

Sebastian Noguera Ruiz − *Department of Chemistry, University of Connecticut, Storrs, Connecticut 06269-3060, United States*

Chao Wang − *Department of Chemistry, University of Connecticut, Storrs, Connecticut 06269-3060, United States;* orcid.org/0009-0007-0698-8477

Haiyan Tan − *Institute of Materials Science, University of Connecticut, Storrs, Connecticut 06269-3136, United States*

Steven L. Suib − *Department of Chemistry, University of Connecticut, Storrs, Connecticut 06269-3060, United States; Department of Materials Science and Engineering and Institute of Materials Science, University of Connecticut, Storrs, Connecticut 06269-3136, United States;* orcid.org/0000-0003-3073-311X

Guoxiang Hu − *School of Materials Science and Engineering, Georgia Institute of Technology, Atlanta, Georgia 30332, United States*

Complete contact information is available at: https://pubs.acs.org/10.1021/acsanm.4c02169

Author Contributions

T.K.T.T. and J.Z. developed the project and designed the experiments. T.K.T.T. performed all the synthesis, optical measurements, TEM, FTIR, and XRD characterization and stability tests. H.N. performed the PL decay measurements. C.B. and G.H. performed the theoretical studies. S.N.R., T.K.T.T., and S.S. performed XPS analysis. T.K.T.T., C.W., and H.T. performed TEM measurements. The manuscript was written through contributions of all authors. All authors have given approval to the final version of the manuscript.

Funding

NSF CHE- 2203854

Notes

The authors declare no competing financial interest.

ACKNOWLEDGMENTS

J.Z. acknowledges the financial support from National Science Foundation (CHE- 2203854) for this project.

REFERENCES

(1) Hao, M.; Bai, Y.; Zeiske, S.; Ren, L.; Liu, J.; Yuan, Y.; Zarrabi, N.; Cheng, N.; Ghasemi, M.; Chen, P.; Lyu, M.; He, D.; Yun, J.-H.; Du, Y.; Wang, Y.; Ding, S.; Armin, A.; Meredith, P.; Liu, G.; Cheng, H.-M.; Wang, L. Ligand-Assisted Cation-Exchange Engineering for High-Efficiency Colloidal Cs1-xFAxPbI3 Quantum Dot Solar Cells with Reduced Phase Segregation. *Nat. Energy* **2020**, *5* (1), 79−88.

(2) Ramasamy, P.; Lim, D.-H.; Kim, B.; Lee, S.-H.; Lee, M.-S.; Lee, J.-S. All-Inorganic Cesium Lead Halide Perovskite Nanocrystals for Photodetector Applications. *Chem. Commun.* **2016**, *52* (10), 2067−2070.

(3) Kovalenko, M. V.; Protesescu, L.; Bodnarchuk, M. I. Properties and Potential Optoelectronic Applications of Lead Halide Perovskite Nanocrystals. *Science (1979)* **2017**, *358* (6364), 745−750.

(4) Kim, Y.-H.; Kim, S.; Kakekhani, A.; Park, J.; Park, J.; Lee, Y.-H.; Xu, H.; Nagane, S.; Wexler, R. B.; Kim, D.-H.; Jo, S. H.; Martínez-Sarti, L.; Tan, P.; Sadhanala, A.; Park, G.-S.; Kim, Y.-W.; Hu, B.; Bolink, H. J.; Yoo, S.; Friend, R. H.; Rappe, A. M.; Lee, T.-W. Comprehensive Defect Suppression in Perovskite Nanocrystals for High-Efficiency Light-Emitting Diodes. *Nat. Photonics* **2021**, *15* (2), 148−155.

(5) Chiba, T.; Hayashi, Y.; Ebe, H.; Hoshi, K.; Sato, J.; Sato, S.; Pu, Y.-J.; Ohisa, S.; Kido, J. Anion-Exchange Red Perovskite Quantum Dots with Ammonium Iodine Salts for Highly Efficient Light-Emitting Devices. *Nat. Photonics* **2018**, *12* (11), 681−687.

(6) Pan, J.; Zhao, Z.; Fang, F.; Wang, L.; Wang, G.; Liu, C.; Huang, Q.; Sun, J.; Huang, Y.; Mao, L.; Xie, J.; Xue, Y.; Chen, J.; Lei, W. A Synergetic Codoping Strategy Enabling Performance Improvement of Pure-Blue Perovskite Quantum Dots Light-Emitting Diodes. *Adv. Opt Mater.* **2022**, *10* (9), 2102569.

(7) Worku, M.; Ben-Akacha, A.; Sridhar, S.; Frick, J. R.; Yin, S.; He, Q.; Robb, A. J.; Chaaban, M.; Liu, H.; Winfred, J. S. R. V.; Hanson, K.; So, F.; Dougherty, D.; Ma, B. Band Edge Control of Quasi-2D Metal Halide Perovskites for Blue Light-Emitting Diodes with Enhanced Performance. *Adv. Funct Mater.* **2021**, *31* (45), 2103299.

(8) Shamsi, J.; Urban, A. S.; Imran, M.; de Trizio, L.; Manna, L. Metal Halide Perovskite Nanocrystals: Synthesis, Post-Synthesis Modifications, and Their Optical Properties. *Chem. Rev.* **2019**, *119* (5), 3296−3348.

(9) Yao, E.-P.; Yang, Z.; Meng, L.; Sun, P.; Dong, S.; Yang, Y.; Yang, Y. High-Brightness Blue and White LEDs Based on Inorganic Perovskite Nanocrystals and Their Composites. *Adv. Mater.* **2017**, *29* (23), 1606859.

(10) Li, G.; Rivarola, F. W. R.; Davis, N. J. L. K.; Bai, S.; Jellicoe, T. C.; de la Peña, F.; Hou, S.; Ducati, C.; Gao, F.; Friend, R. H.; Greenham, N. C.; Tan, Z.-K. Highly Efficient Perovskite Nanocrystal Light-Emitting Diodes Enabled by a Universal Crosslinking Method. *Adv. Mater.* **2016**, *28* (18), 3528−3534.

(11) Lignos, I.; Protesescu, L.; Emiroglu, D. B.; Maceiczyk, R.; Schneider, S.; Kovalenko, M. V.; deMello, A. J. Unveiling the Shape Evolution and Halide-Ion-Segregation in Blue-Emitting Formamidinium Lead Halide Perovskite Nanocrystals Using an Automated Microfluidic Platform. *Nano Lett.* **2018**, *18* (2), 1246−1252.

(12) Protesescu, L.; Yakunin, S.; Bodnarchuk, M. I.; Krieg, F.; Caputo, R.; Hendon, C. H.; Yang, R. X.; Walsh, A.; Kovalenko, M. V. Nanocrystals of Cesium Lead Halide Perovskites (CsPbX3, X = Cl, Br, and I): Novel Optoelectronic Materials Showing Bright Emission with Wide Color Gamut. *Nano Lett.* **2015**, *15* (6), 3692−3696.

(13) Kong, X.; Wu, Y.; Xu, F.; Yang, S.; Cao, B. Ultrasmall CsPbBr3 Quantum Dots with Bright and Wide Blue Emissions. *physica status solidi (RRL) - Rapid Research Letters* **2021**, *15* (7), 2100134.

(14) Liu, H.; Worku, M.; Mondal, A.; Shonde, T. B.; Chaaban, M.; Ben-Akacha, A.; Lee, S.; Gonzalez, F.; Olasupo, O.; Lin, X.; Vellore Winfred, J. S. R.; Xin, Y.; Lochner, E.; Ma, B. Efficient and Stable Blue Light Emitting Diodes Based on CsPbBr3 Nanoplatelets with Surface Passivation by a Multifunctional Organic Sulfate. *Adv. Energy Mater.* **2022**, *13*, 2201605.

(15) Zhang, C.; Wan, Q.; Wang, B.; Zheng, W.; Liu, M.; Zhang, Q.; Kong, L.; Li, L. Surface Ligand Engineering toward Brightly Luminescent and Stable Cesium Lead Halide Perovskite Nanoplatelets for Efficient Blue-Light-Emitting Diodes. *J. Phys. Chem. C* **2019**, *123* (43), 26161−26169.

(16) Wang, H.; Ye, F.; Sun, J.; Wang, Z.; Zhang, C.; Qian, J.; Zhang, X.; Choy, W. C. H.; Sun, X. W.; Wang, K.; Zhao, W. Efficient CsPbBr3 Nanoplatelet-Based Blue Light-Emitting Diodes Enabled by Engineered Surface Ligands. *ACS Energy Lett.* **2022**, *7* (3), 1137−1145.

(17) Akkerman, Q. A.; Motti, S. G.; Srimath Kandada, A. R.; Mosconi, E.; D'Innocenzo, V.; Bertoni, G.; Marras, S.; Kamino, B. A.; Miranda, L.; De Angelis, F.; Petrozza, A.; Prato, M.; Manna, L. Solution Synthesis Approach to Colloidal Cesium Lead Halide Perovskite Nanoplatelets with Monolayer-Level Thickness Control. *J. Am. Chem. Soc.* **2016**, *138* (3), 1010−1016.
(18) Bohn, B. J.; Tong, Y.; Gramlich, M.; Lai, M. L.; Döblinger, M.; Wang, K.; Hoye, R. L. Z.; Müller-Buschbaum, P.; Stranks, S. D.; Urban, A. S.; Polavarapu, L.; Feldmann, J. Boosting Tunable Blue Luminescence of Halide Perovskite Nanoplatelets through Post-synthetic Surface Trap Repair. *Nano Lett.* **2018**, *18* (8), 5231−5238.
(19) Burlakov, V. M.; Hassan, Y.; Danaie, M.; Snaith, H. J.; Goriely, A. Competitive Nucleation Mechanism for CsPbBr3 Perovskite Nanoplatelet Growth. *J. Phys. Chem. Lett.* **2020**, *11* (16), 6535−6543.
(20) Almeida, G.; Goldoni, L.; Akkerman, Q.; Dang, Z.; Khan, A. H.; Marras, S.; Moreels, I.; Manna, L. Role of Acid-Base Equilibria in the Size, Shape, and Phase Control of Cesium Lead Bromide Nanocrystals. *ACS Nano* **2018**, *12* (2), 1704−1711.
(21) De Roo, J.; Ibáñez, M.; Geiregat, P.; Nedelcu, G.; Walravens, W.; Maes, J.; Martins, J. C.; Van Driessche, I.; Kovalenko, M. V.; Hens, Z. Highly Dynamic Ligand Binding and Light Absorption Coefficient of Cesium Lead Bromide Perovskite Nanocrystals. *ACS Nano* **2016**, *10* (2), 2071−2081.
(22) DuBose, J. T.; Christy, A.; Chakkamalayath, J.; Kamat, P. V. Transformation of Perovskite Nanoplatelets to Large Nanostructures Driven by Solvent Polarity. *ACS Mater. Lett.* **2022**, *4* (1), 93−101.
(23) Wang, Y.; Li, X.; Sreejith, S.; Cao, F.; Wang, Z.; Stuparu, M. C.; Zeng, H.; Sun, H. Photon Driven Transformation of Cesium Lead Halide Perovskites from Few-Monolayer Nanoplatelets to Bulk Phase. *Adv. Mater.* **2016**, *28* (48), 10637−10643.
(24) Dang, Z.; Dhanabalan, B.; Castelli, A.; Dhall, R.; Bustillo, K. C.; Marchelli, D.; Spirito, D.; Petralanda, U.; Shamsi, J.; Manna, L.; Krahne, R.; Arciniegas, M. P. Temperature-Driven Transformation of CsPbBr3 Nanoplatelets into Mosaic Nanotiles in Solution through Self-Assembly. *Nano Lett.* **2020**, *20* (3), 1808−1818.
(25) Shamsi, J.; Kubicki, D.; Anaya, M.; Liu, Y.; Ji, K.; Frohna, K.; Grey, C. P.; Friend, R. H.; Stranks, S. D. Stable Hexylphosphonate-Capped Blue-Emitting Quantum-Confined CsPbBr3 Nanoplatelets. *ACS Energy Lett.* **2020**, *5* (6), 1900−1907.
(26) Zhang, X.; Zhou, Y.; Peng, L.; Lin, Z.; Chang, Y.; Zhou, Z.; Li, Y. Stable Blue-Emitting CsPbBr3 Nanoplatelets for Lighting and Display Applications. *ACS Appl. Nano Mater.* **2022**, *5* (11), 17012−17021.
(27) Wang, S.; Wang, W.; Donmez, S.; Xin, Y.; Mattoussi, H. Engineering Highly Fluorescent and Colloidally Stable Blue-Emitting CsPbBr3 Nanoplatelets Using Polysalt/PbBr2 Ligands. *Chem. Mater.* **2022**, *34* (11), 4924−4936.
(28) Kresse, G.; Furthmüller, J. Efficiency of Ab-Initio Total Energy Calculations for Metals and Semiconductors Using a Plane-Wave Basis Set. *Comput. Mater. Sci.* **1996**, *6* (1), 15−50.
(29) Kresse, G.; Furthmüller, J. Efficient Iterative Schemes for Ab Initio Total-Energy Calculations Using a Plane-Wave Basis Set. *Phys. Rev. B* **1996**, *54* (16), 11169−11186.
(30) Perdew, J. P.; Burke, K.; Ernzerhof, M. Generalized Gradient Approximation Made Simple. *Phys. Rev. Lett.* **1996**, *77* (18), 3865−3868.
(31) Blöchl, P. E. Projector Augmented-Wave Method. *Phys. Rev. B* **1994**, *50* (24), 17953−17979.
(32) Liu, P.; Chen, W.; Wang, W.; Xu, B.; Wu, D.; Hao, J.; Cao, W.; Fang, F.; Li, Y.; Zeng, Y.; Pan, R.; Chen, S.; Cao, W.; Sun, X. W.; Wang, K. Halide-Rich Synthesized Cesium Lead Bromide Perovskite Nanocrystals for Light-Emitting Diodes with Improved Performance. *Chem. Mater.* **2017**, *29* (12), 5168−5173.
(33) Wu, Y.; Wei, C.; Li, X.; Li, Y.; Qiu, S.; Shen, W.; Cai, B.; Sun, Z.; Yang, D.; Deng, Z.; Zeng, H. In Situ Passivation of PbBr64-Octahedra toward Blue Luminescent CsPbBr3 Nanoplatelets with Near 100% Absolute Quantum Yield. *ACS Energy Lett.* **2018**, *3* (9), 2030−2037.
(34) Imran, M.; Ijaz, P.; Goldoni, L.; Maggioni, D.; Petralanda, U.; Prato, M.; Almeida, G.; Infante, I.; Manna, L. Simultaneous Cationic and Anionic Ligand Exchange For Colloidally Stable CsPbBr3 Nanocrystals. *ACS Energy Lett.* **2019**, *4* (4), 819−824.
(35) Yin, W.; Li, M.; Dong, W.; Luo, Z.; Li, Y.; Qian, J.; Zhang, J.; Zhang, W.; Zhang, Y.; Kershaw, S. V.; Zhang, X.; Zheng, W.; Rogach, A. L. Multidentate Ligand Polyethylenimine Enables Bright Color-Saturated Blue Light-Emitting Diodes Based on CsPbBr3 Nanoplatelets. *ACS Energy Lett.* **2021**, *6* (2), 477−484.
(36) He, H.; Yu, Q.; Li, H.; Li, J.; Si, J.; Jin, Y.; Wang, N.; Wang, J.; He, J.; Wang, X.; Zhang, Y.; Ye, Z. Exciton Localization in Solution-Processed Organolead Trihalide Perovskites. *Nat. Commun.* **2016**, *7* (1), 10896.
(37) Li, J.; Gan, L.; Fang, Z.; He, H.; Ye, Z. Bright Tail States in Blue-Emitting Ultrasmall Perovskite Quantum Dots. *J. Phys. Chem. Lett.* **2017**, *8* (24), 6002−6008.
(38) Pan, A.; He, B.; Fan, X.; Liu, Z.; Urban, J. J.; Alivisatos, A. P.; He, L.; Liu, Y. Insight into the Ligand-Mediated Synthesis of Colloidal CsPbBr3 Perovskite Nanocrystals: The Role of Organic Acid, Base, and Cesium Precursors. *ACS Nano* **2016**, *10* (8), 7943−7954.
(39) Ye, J.; Li, Z.; Kubicki, D. J.; Zhang, Y.; Dai, L.; Otero-Martínez, C.; Reus, M. A.; Arul, R.; Dudipala, K. R.; Andaji-Garmaroudi, Z.; Huang, Y.-T.; Li, Z.; Chen, Z.; Müller-Buschbaum, P.; Yip, H.-L.; Stranks, S. D.; Grey, C. P.; Baumberg, J. J.; Greenham, N. C.; Polavarapu, L.; Rao, A.; Hoye, R. L. Z. Elucidating the Role of Antisolvents on the Surface Chemistry and Optoelectronic Properties of CsPbBrxI3-x Perovskite Nanocrystals. *J. Am. Chem. Soc.* **2022**, *144* (27), 12102−12115.
(40) Dou, L.; Wong, A. B.; Yu, Y.; Lai, M.; Kornienko, N.; Eaton, S. W.; Fu, A.; Bischak, C. G.; Ma, J.; Ding, T.; Ginsberg, N. S.; Wang, L.-W.; Alivisatos, A. P.; Yang, P. Atomically Thin Two-Dimensional Organic-Inorganic Hybrid Perovskites. *Science (1979)* **2015**, *349* (6255), 1518−1521.
(41) Gao, H.; Feng, W.; Liu, H.; Liu, S.; Wang, Z.; Yao, D.; Liu, Y.; Teng, D.-K.; Yang, B.; Zhang, H. Cesium-Lead Bromide Perovskite Nanoribbons with Two-Unit-Cell Thickness and Large Lateral Dimension for Deep-Blue Light Emission. *ACS Appl. Nano Mater.* **2020**, *3* (5), 4826−4836.
(42) Zhang, X.; Bai, X.; Wu, H.; Zhang, X.; Sun, C.; Zhang, Y.; Zhang, W.; Zheng, W.; Yu, W. W.; Rogach, A. L. Water-Assisted Size and Shape Control of CsPbBr3 Perovskite Nanocrystals. *Angew. Chem., Int. Ed.* **2018**, *57* (13), 3337−3342.
(43) Fu, W.; Yang, H.; Chang, L.; Li, M.; Bala, H.; Yu, Q.; Zou, G. Preparation and Characteristics of Core-Shell Structure Nickel/Silica Nanoparticles. *Colloids Surf. A Physicochem Eng. Asp* **2005**, *262* (1), 71−75.
(44) Hardikar, V. V.; Matijević, E. Coating of Nanosize Silver Particles with Silica. *J. Colloid Interface Sci.* **2000**, *221* (1), 133−136.
(45) Vogt, C.; Toprak, M. S.; Muhammed, M.; Laurent, S.; Bridot, J.-L.; Müller, R. N. High Quality and Tuneable Silica Shell-Magnetic Core Nanoparticles. *J. Nanopart. Res.* **2010**, *12* (4), 1137−1147.
(46) El-Toni, A. M.; Yin, S.; Sato, T. Control of Silica Shell Thickness and Microporosity of Titania-Silica Core-Shell Type Nanoparticles to Depress the Photocatalytic Activity of Titania. *J. Colloid Interface Sci.* **2006**, *300* (1), 123−130.
(47) Lu, Y.; McLellan, J.; Xia, Y. Synthesis and Crystallization of Hybrid Spherical Colloids Composed of Polystyrene Cores and Silica Shells. *Langmuir* **2004**, *20* (8), 3464−3470.
(48) Li, M.; Zhang, X.; Yang, P. Controlling the Growth of a SiO2 Coating on Hydrophobic CsPbBr3 Nanocrystals towards Aqueous Transfer and High Luminescence. *Nanoscale* **2021**, *13* (6), 3860−3867.
(49) Meng, C.; Yang, D.; Wu, Y.; Zhang, X.; Zeng, H.; Li, X. Synthesis of Single CsPbBr3@SiO2 Core-Shell Particles via Surface Activation. *J. Mater. Chem. C* **2020**, *8* (48), 17403−17409.
(50) Beal, R. E.; Slotcavage, D. J.; Leijtens, T.; Bowring, A. R.; Belisle, R. A.; Nguyen, W. H.; Burkhard, G. F.; Hoke, E. T.; McGehee,

https://doi.org/10.1021/acsanm.4c02169
ACS Appl. Nano Mater. 2024, 7, 12153−12162

M. D. Cesium Lead Halide Perovskites with Improved Stability for Tandem Solar Cells. *J. Phys. Chem. Lett.* **2016**, *7* (5), 746−751.
(51) Wang, F.; Geng, W.; Zhou, Y.; Fang, H.-H.; Tong, C.-J.; Loi, M. A.; Liu, L.-M.; Zhao, N. Phenylalkylamine Passivation of Organolead Halide Perovskites Enabling High-Efficiency and Air-Stable Photovoltaic Cells. *Adv. Mater.* **2016**, *28* (45), 9986−9992.

https://doi.org/10.1021/acsanm.4c02169
ACS Appl. Nano Mater. 2024, 7, 12153−12162